Cement and Concrete Research 38 (2008) 993–1004

Contents lists available at ScienceDirect

Cement and Concrete Research

journal homepage: http://ees.elsevier.com/CEMCON/default.asp

Mechanical behavior of concretes damaged by alkali-silica reaction

G. Giaccio [a,b,*], R. Zerbino [a,b], J.M. Ponce [a,c], O.R. Batic [a]

[a] LEMIT, Commission of Scientific Research .52 y 121, 1900 La Plata, Argentina
[b] Department of Civil Engineering, La Plata National University.1 y 47, 1900 La Plata, Argentina
[c] Faculty of Natural Science and Museum, La Plata National University. 122 y 60, 1900 La Plata, Argentina

ARTICLE INFO

Article history:
Received 8 September 2006
Accepted 26 February 2008

Keywords:
Alkali-silica reaction
Degradation
Expansion
Mechanical properties
Microcracking

ABSTRACT

Alkali-silica reaction (ASR) can induce the premature distress and loss in serviceability of concrete structures. The internal crack pattern produced by ASR affects both transport and mechanical properties. Usually linear expansions are considered as indicative of the grade of damage into the material (internal crack pattern), nevertheless as diverse types of ASR have been recognized (rapid or slow reactive aggregates, fine or coarse aggregates) the effects on strength and rheological properties could be different for a same expansion. This paper compares the mechanical response of a reference concrete (without reactive aggregates) and concretes prepared with three different types of reactive aggregates, with the same mixture proportions. The first concrete incorporated 10% of a highly reactive siliceous orthoquartzite as a part of the coarse aggregate, the second included a highly reactive sand, and the third prepared with a slow reactive granitic migmatite as coarse aggregate. Concretes were moist cured at 38 °C. When linear expansions ranging between 0.11 and 0.18% took place, the stress strain behavior in compression and the load-displacement response in flexure were measured. The same tests were performed on reference concrete at different ages, between 75 and 745 days. Microscopic observations were performed on polished and thin sections in order to analyze concrete microstructure. It appears that the failure mechanism of concrete in compression is clearly affected by ASR, the shape of the stress–strain curves reflects the presence of internal fissures, showing that the capability of controlling crack propagation decreases. Differences in the crack pattern are also reflected in the shape of the load-deflection curves in tension, damaged concretes show an increased non-linearity and a more gradual softening. However, it was found that the modifications in the mechanical properties cannot be directly associated with a level of expansion, as the behavior depends on the component materials and mechanisms involved in the reaction.

1. Introduction

Alkali-silica reaction (ASR) can induce the premature distress and loss in serviceability of concrete structures. It is generally agreed that ASR occurs in concretes with reactive aggregates, when there are sufficient alkalis (K_2O, Na_2O), and when relative humidity is higher than 85%. In addition, temperature affects the time of initiation (induction period) and development of the reaction. As ASR takes place, different signs appear inside the concrete, gels and cracks form, gels filling cracks in the aggregates or in the cement paste, gels form reaction rims around aggregate particles, gels fill air-voids in the cement paste and silica gels replacing C–S–H of hydrated cement paste [1,2].

ASR has been studied for more than 70 years and has been reported in more than 50 countries around the world [3,4]. In Argentina more than 100 examples of structures, placed in regions with different climates, damaged by ASR have been reported since 1950 [5].

The mineralogical structure of the aggregates is one of the main factors affecting ASR, amorphous silica (opal), chalcedony, cristobalite, tridymite and volcanic glass appear as the reactive components leading to a rapid or normal reaction rate, showing visible signs of reaction in concrete at ages as low as 1 year, depending on the surrounding environment. Other aggregates as those composed by granitic and metamorphic rocks, that include mineral species as polycrystalline and strained quartz, need very long induction periods usually higher than 10 years [6–8]. Different levels of damage and cracking appear in concrete microstructure according to the kinetic of ASR [9]. Rapid reaction rates induce internal stresses at the interfaces and cement pastes, producing micro and macrocraks. On the other hand in concretes with strained quartz, the reactions are localized inside the aggregates in reactive zones (intercrystals), where pore solution can reach. This process takes place very slowly and the attack is not generalized all around the aggregate surface [9].

Many authors have studied the effect of ASR on the mechanical properties of plain and reinforced concrete [10–15]. Most of them agree that ASR strongly affects concrete tensile strength and the modulus of elasticity. The reductions in compressive strength are always lower than those observed in stiffness, being in some cases

* Corresponding author. LEMIT, Commission of Scientific Research .52 y 121, 1900 La Plata, Argentina. Tel.: +54 221 483 1142/44; fax: +54 221 4250471.
E-mail address: ggiaccio@ing.unlp.edu.ar (G. Giaccio).

0008-8846/$ – see front matter © 2008 Elsevier Ltd. All rights reserved.
doi:10.1016/j.cemconres.2008.02.009

Table 1
Physical and chemical characteristics of the cement

Physical properties			
Retained # 75 μm (%)			4.0
Specific surface area Blaine m^2/kg			348
Water for normal consistency (%)			23.0
Setting time (h:m)			
Initial			2:45
Final			3:30
Compressive strength (MPa)			
2 days			32.8
7 days			53.2
28 days			54.3
90 days			55.7
Autoclave expansion (%)			−0.02
Chemical analysis			
SO_3 (%)	2.1	Na_2O (%)	0.09
CaO (%)	65.5	K_2O (%)	0.96
MgO (%)	0.63	Total alkali (Na_2O_e)	0.72
Fe_2O_3 (%)	4.20	Loss on ignition (%)	1.60
SiO_2 (%)	21.0	Insoluble residue (%)	0.40
Al_2O_3 (%)	3.40		

compressive strength even not affected. Then compressive strength is not necessarily a good indicator of the quality of concrete damaged by ASR. In this sense the analysis of the failure mechanism in ASR concrete becomes more relevant.

A research project was performed with the aim of analyzing the effects of ASR on the behavior of concrete. In this paper the mechanical responses of a reference concrete and three ASR affected concretes are compared. The mechanical behavior in tension and compression was recorded when comparable linear expansions took place in each ASR damaged concrete. In addition petrographic and microstructural analyses on polished and thin sections were performed in order to characterize the damage.

2. Experimental

2.1. Materials and mixtures

Three concretes damaged by ASR were selected, based on previous experience on local materials [16–18], with the purpose of comparing the failure mechanism in tension and compression of concretes with similar expansion levels but different morphology of defects (location, size and type of cracks). The main characteristics and the identification of the aggregates are summarized as follows.

Coarse aggregate A: Very reactive siliceous orthoquartzite obtained from Chaco province, Argentina. This compact fine to medium-grained rock consists of quartz grains embedded in a groundmass of opal, chalcedony and microcrystalline quartz. Opal and chalcedony making up the cement matrix of this rock are responsible for the reactivity of this aggregate. Normalized expansion tests (ASTM C 1293, concrete prisms) indicate an expansion of 0.190% at 1 year. Tests in accordance with ASTM C 1260 indicate expansions of 0.380% at 16 days.

Coarse aggregate B: Slow reactive granitic crushed stone obtained from an active quarry at Buenos Aires province, Argentina. This rock is composed by feldspars (orthoclase and plagioclase), quartz, micas, epidote, zircon and dark minerals. Strained quartz grains show undulatory extinction. It can be classified as cataclastic granitic migmatite. Expansion tests (ASTM C 1293, concrete prisms) indicate an expansion of 0.070% at 1 year. Tests in accordance with ASTM C 1260 indicate expansions of 0.162% at 16 days.

Coarse aggregate C: Non-reactive granitic crushed stone (Buenos Aires province, Argentina). It consists of two types of rock, 98.5% of granitic migmatite and 1.5% of amphibolite. The former is reddish grey, medium grained, compact and inaltered. From microscopic observations it exhibits a granoblastic texture consisting of quartz with crystal size ranging between 0.8 and 1.4 mm, some of which show undulatory extinction, plagioclase, amphiboles, mica, apatite and magnetite. Tested in accordance with ASTM C 1293 and C 1260, this aggregate gives expansions 0.025% and 0.070% respectively, below the threshold value to be considered deleterious. The structures where it has been used show excellent performance both in strength and durability.

Fine aggregate D: Reactive sand obtained from an active bed at Rio Negro province, Argentina. This lithic sand is mainly composed of andesitic–rhyolitic clasts which contains vitreous groundmass, and bioclasts having amorphous and cryptocrystalline silica (opal and chalcedony). Expansion tests according to ASTM C 1293 and C 1260 indicate expansions of 0.525% at 1 year and 0.462% at 16 days respectively.

Fine aggregate E: Non-reactive natural sand obtained from the east coast of La Plata River, Argentina. It has rounded particles composed by quartz (>70%), lithic granitic fragments, feldspars (plagioclase), pyroxenes and a very little content (0.5%) of chalcedony. Expansion tests according to ASTM C 1293 and C 1260 indicate expansions of 0.038% at 1 year and 0.080% at 16 days respectively.

A high alkali ordinary Portland cement was used; its physical and chemical characteristics are given in Table 1.

Four concretes were prepared adding NaOH (as granular particles) in the mixing water to achieve a total alkali in concrete of 5.25 kg/m^3 Na_2O_e. Coarse aggregate particle size ranged between 5 and 19 mm, distributed in 3 equal fractions in accordance with ASTM C 1293. The control concrete (C1) was prepared with the non-reactive natural siliceous sand E and the granitic crushed stone C. In concrete R2 the non-reactive sand was replaced by the reactive sand D. Concrete R3 incorporated 10% of the very reactive siliceous orthoquartzite A and 90% of the aggregate C as coarse aggregate. Finally concrete R4 was prepared including 100% of the slow reactive granitic crushed stone B as coarse aggregate. The mixture proportions and the properties of fresh concrete are given in Table 2.

Table 2
Mixture proportions (kg/m^3) and properties of fresh concrete

Concrete	C1	R2	R3	R4
W/C ratio	0.42			
Water	176			
Cement	420			
Total alkali in concrete (Na_2O_e)	5.25			
Reactive siliceous orthoquartzite (A)	–	–	120	–
Slow reactive granitic crushed stone (B)	–	–	–	1090
Non-reactive granitic crushed stone (C)	1090	1090	980	–
Natural reactive sand (D)	–	710	–	–
Non-reactive natural sand (E)	710	–	710	710
Slump (mm)	160	135	160	135
Air content (%)	2.8	2.4	2.5	2.3
Concrete temperature (°C)	24.6	25.3	25.5	25.3

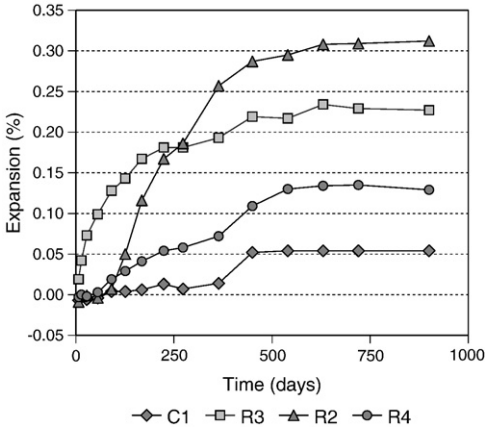

Fig. 1. Linear expansions.

Table 3
Testing program

Concrete	Age (days)	Linear expansion[a] (%)	$f'c$, E	$f'c$, E, f_{crit}, f_{init} and Poisson's ratio	Load-deflection and load-CMOD curves
	Specimen type	75×75 mm prisms	100×200 mm cylinders	150×300 mm cylinders	75×105 mm prisms
C1	28	−0.006	X	–	–
	75	0.004	X	X	X
	250	0.007	X	X	X
	745	0.054	X	X	X
R2	28	−0.001	X	–	–
	200	0.145	X	X	X
	250	0.180	X	X	X
R3	28	0.073	X	–	–
	75	0.115	X	X	X
	120	0.145	X	X	X
R4	28	−0.002	X	–	–
	485	0.125	X	X	X
	745	0.135	X	X	X

[a] Interpolated from Fig. 1.

2.2. Test methods and testing program

Prisms and cylinders were cast. All of them were compacted by external vibration and kept protected after casting to avoid water evaporation. After 24 h they were covered with a cotton sheet and placed inside plastic bags, including 5 ml of water. These bags were stored at 38 °C. Before reading, the specimens were stored 24 h at 21 ± 1 °C in the laboratory maintaining the cotton sheet, and then they were tested in a saturated condition.

Linear expansions were measured as a way to evaluate the ASR process. When concretes R2 to R4 achieved linear expansions in the order of 0.11 and 0.18%, the following tests were performed: 1) stress–strain behavior in compression, 2) load-displacement and load-crack mouth opening displacement (CMOD) behavior in flexure on notched beams and 3) optical and microscopic observations on concrete slices. Concrete (C1) was tested at three ages between 75 and 745 days; to consider the evolution of concrete properties with time.

Expansion measurements were performed in accordance with ASTM C 1293, with a precision of 0.00254 mm. Two sizes of specimens were used, 75×75×300 mm and 75×105×430 mm, the first is usually adopted to follow the length changes while the last ones were selected to perform the flexural tests.

Uniaxial compression tests were performed on cylinders of 150×300 mm. Three loading–unloading cycles, up to 40% of the maximum stress, were applied to determine the modulus of elasticity and Poisson's ratio (ASTM C 469), after which the load was increased monotonically up to failure. A controlled closed loop system was used being the axial deformation of the control signal. In addition the lateral deformations

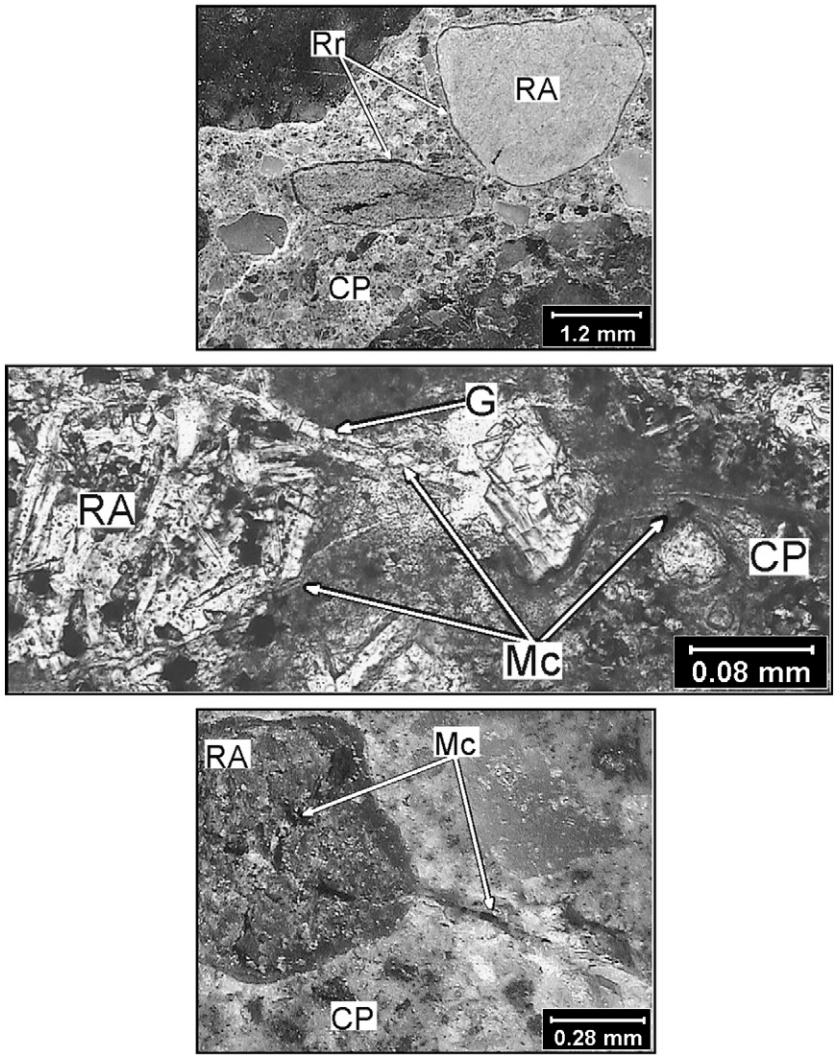

Fig. 2. Microscopic observations of concrete R2. RA: reactive aggregate, Rr: reaction rim, Mc: microcrack, CP: cement paste, G: gel. a. (top) Reaction rim in two reactive fine aggregates. Polished section viewed with a stereo-zoom microscope. b. (centre) Development of microcracks filled with gel. Thin section viewed through parallel polarizers. c. (bottom) Reactive fine aggregate showing a higher degree of deterioration. Polished section viewed with a stereobinocular microscope.

were measured. The development of the failure process under compressive loads was followed by means of the analysis of the stress–strain curves. Based on them, the initiation (f_{init}) and critical (f_{crit}) stresses can be obtained, representing the starting of matrix crack growth and the onset of unstable propagation of cracks in concrete [19]. Complementary cylinders of 100×200 mm were used to evaluate the compressive strength and modulus of elasticity at 28 days and their evolutions.

Three-point bending tests of middle notched specimens were performed to study the stress–strain behavior in tension. The notch was cut up to a depth equal to half of the beam's height 1 day before testing, using a diamond saw. A controlled closed loop system was used, the beams were loaded over a span of 400 mm and the tests were controlled by the average of the central deflection. In addition, CMOD (crack mouth opening displacement) at the notch was measured. The net bending stress at maximum load (f_{net}) and the fracture energy (G_F) were obtained from the load-deflection curves following the general guidelines of the RILEM 50-FMC Committee [20]. Weight-compensated flexural tests were made [21], consequently it was not necessary to consider the contribution of the self weight of the beams (mg) in the fracture process. The energy of fracture was calculated as $G_F = W_0/A_{lig}$ where W_0 is the work of fracture (equal to the area below the load-deflection plot) and A_{lig} the cross-sectional area of the ligament before the test. The net bending stress at maximum load was calculated as $f_{net} = 6\ F_{max}\ l/4\ bh^2$ where b is the beam width, h the net depth of the beam, l the span and F_{max} the maximum load. Finally the characteristic length, parameter representative of the size of the fracture zone, was calculated as $l_{ch} = EG_F/f_s^2$ using the values of the modulus of elasticity (E) obtained from 150×300 mm cylinder tests and the tensile strength (f_s) estimated as $0.6\ f_{net}$ [22].

Before the flexural and compressive tests the specimen's surfaces were carefully examined with the aim to identify the presence of gels, stains and cracks. Afterwards stereo-zoom microscope observations on polished sections of concrete and polarizing microscope observations on thin sections of prisms were made. To obtain polished section slices of 100×75×10 mm were cut and polished until a specular surface was obtained; they were carefully washed to avoid losing reaction products. Thin sections were prepared cutting a 75×50×5 mm sample, then it was glued to a slide and the concrete slice was then reduced in thickness until approximately 30 μm.

3. Results

3.1. Linear expansion and cracking morphology

The ages of testing were adopted according to the level of expansion achieved. Fig. 1 gives the linear expansions measured on

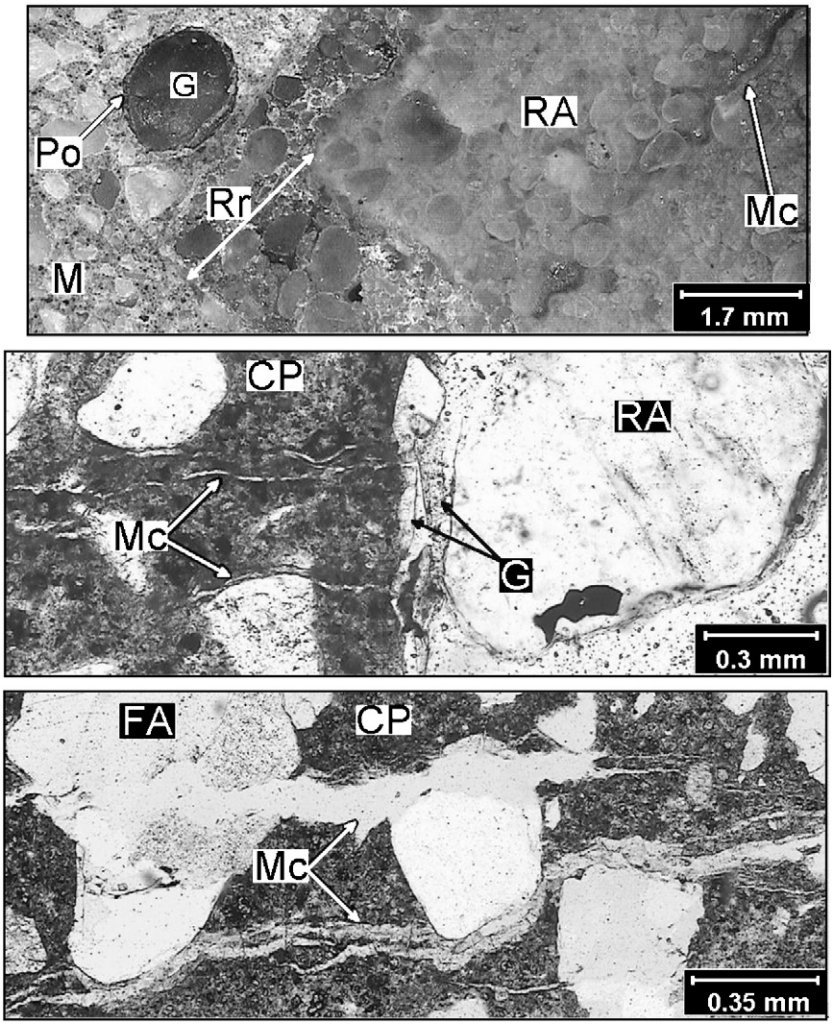

Fig. 3. Microscopic observations of concrete R3. RA: reactive aggregate, FA: fine aggregate, Rr: reaction rim, Mc: microcrack, CP: cement paste, M: mortar, G: gel, Po: pore. a. (top) Microstructures developed by the alkali-silica reaction. Polished section viewed with a stereo-zoom microscope. b. (centre) Appearance of microcracking in the interfacial zone adjacent to reactive aggregate. Thin section viewed through parallel polarizers. c. (bottom) Microcracks filled with gel running through interfaces and cement paste. Thin section viewed through parallel polarizers.

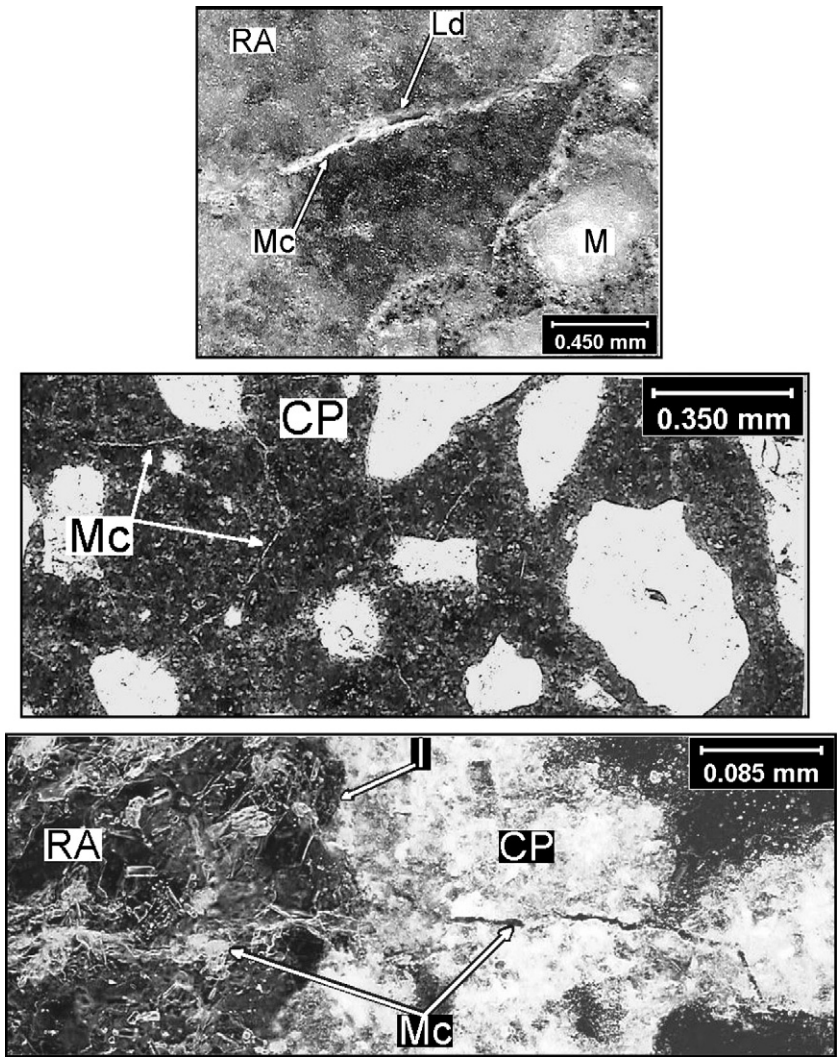

Fig. 4. Microscopic observations of concrete R4. RA: reactive aggregate, Ld: local dissolution, Mc: microcrack, CP: cement paste, M: mortar, I: interfaces. a. (top) Local dissolution in a microcrack of a reactive aggregate. Polished section viewed with a stereo-zoom microscope. b. (centre) Internal microcrack pattern in the cement paste. Thin section viewed through parallel polarizers. c. (bottom) Microcrack running from reactive aggregate toward the cement paste. Thin section viewed through parallel polarizers and inverted light.

the 75×75×300 mm prisms. It can be seen that concrete R3 presents an important expansion during the first weeks, and that the expansion rate decreases after 150 days. Different behaviors show R2 and R4. Concrete R2 has an induction period of near 100 days, and then it presents an important reactivity up to 450 days which leads to expansions near 0.300%. Concrete R4 shows a slow expansion rate, after 550 days it achieves stable values of expansion near 0.130%. These expansions are in accordance with those measured up to testing age on 75×105×430 mm beams, which were cast for flexural tests.

Table 3 summarizes the testing program including the age and the corresponding linear expansion of each concrete. Concrete R3 has a significant expansion at 75 days, being possible to observe fissures at the surface of the specimens. At 120 days the degree of cracking was very important, then this concrete was tested at the ages of 28, 75 and

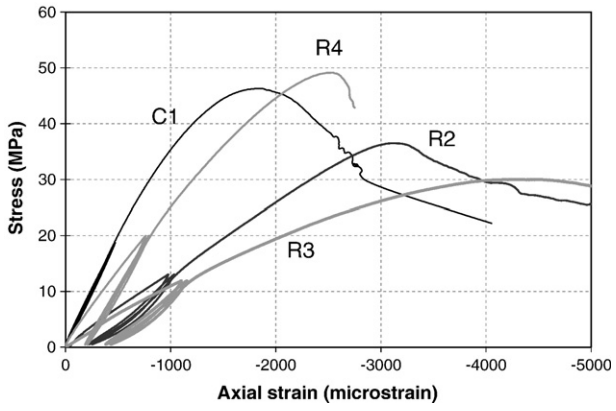

Fig. 5. Stress–strain curves in compression of damaged and control concretes.

Table 4
Typical characteristics of the crack pattern obtained from microscope observations

Concrete		Cement paste		Interfaces		Aggregates	
		TL	MW	TL	MW	TL	MW
		(mm/cm^2)	(mm)	(mm/cm^2)	(mm)	(mm/cm^2)	(mm)
R2		2.0	0.10	1.1	0.05	0.33	0.05
R3		3.5	0.20	2.7	0.05	1.1	0.02
				Reaction rims	2		
R4	Thin	90	0.009	0.75	0.03	1.8	0.05
	Wide	0.7	0.025				

TL = Total microcrack length per unit area.
MW = Maximum microcrack width.

Table 5
Compression test results

Concrete	Age (days)	$f'c$ (MPa)	E (GPa)	$f'c$ (MPa)	E (GPa)	f_{crit} (MPa)	f_{crit} (%)	f_{init} (MPa)	f_{init} (%)	Poisson's ratio	Expansion[a] (%)
	Specimen type	Cylinders (diameter-height)									Prisms
		100×200 mm		150×300 mm							75×75 mm
C1	28	28.6 (4)[b]	35.7	–	–	–	–	–	–	–	−0.006
	75	39.5 (1)	38.2	39.1 (4)[b]	38.7	37.6	96	33.2	85	0.19	0.004
	250	47.4 (3)	37.9	46.2 (2)	39.7	44.5	96	38.1	83	0.22	0.007
	745	49.4 (8)	37.4	47.6 (9)	39.6	44.8	94	40.5	85	0.22	0.054
R2	28	27.8 (11)	32.0	–	–	–	–	–	–		−0.001
	200	37.8 (16)	17.1	37.3 (6)	19.9	29.6	79	24.2	65	0.18	0.145
	250	29.1 2)	13.1	33.6 (8)	12.1	22.5	67	20.6	61	0.19	0.180
R3	28	30.2 (9)	24.1	–	–	–	–	–	–	–	0.073
	75	30.8 (11)	25.1	28.9 (14)	19.0	17.6	61	15.9	55	0.17	0.115
	120	32.8 (3)	21.7	29.7 (8)	18.4	20.7	70	16.6	56	0.11	0.145
R4	28	36.5 (6)	38.1	–	–	–	–	–	–	–	−0.002
	485	51.2 (5)	31.3	49.8 (5)	33.0	48.8	98	41.5	83	0.22	0.125
	745	48.2 (2)	30.1	49.7 (7)	28.8	46.0	93	38.4	77	0.21	0.135

$f'c$: Compressive strength.
E: Modulus of elasticity.
f_{crit}: Critical stress.
f_{init}: Initiation stress.
[a] Interpolated from Fig. 1 data.
[b] COV (%).

120 days. Expansion levels near 0.120%, took place in concretes R2 and R4 after 6 and 16 months respectively. Concrete C1 was tested at 28, 75, 250 and 745 days in order to evaluate the evolution of the mechanical properties along the whole period of the study.

Figs. 2–4 show stereo-zoom and polarizing microscope observations made on slices of concretes R2 to R4. The main morphologic characteristics of the concretes associated to the ASR process are discussed.

As was said concrete R2 is composed by a non-reactive granitic coarse aggregate (C) and a reactive natural sand (D). The potential reactive mineralogical species are volcanic glass and perhaps polymorphous of silica (trydimite–cristobalite) that is present in small volcanic clasts, where clear deleterious signs are observed. With this type of reactive aggregate, reaction usually takes place at the interfaces around the aggregates, forming dark rings filled with gel. It is assumed that important gel pressures will develop in these concretes. The fissures, filled with gel, start at the interfaces and run into the bulk cement paste leading to a diffuse crack pattern. Eventually there appear some cracks into the reactive aggregates. Fig. 2 presents selected photograph of samples of concrete R2 illustrating the reaction characteristics. Fig. 2a shows one of the most characteristic signs of this reaction, the reaction rims at the interfaces where a kind of dark ring around the affected grains appear. In addition, microcracks are generated from the gels expansion into the reactive fine aggregate that afterwards grow into the cement paste. At the age of 7 months prevalent microcracks develop irregular shapes with apertures ranging between 0.005 and 0.02 mm; most of them are filled with gel that appears transparent, colorless and massive as shown in Fig. 2b. A diffused microcracking through whole

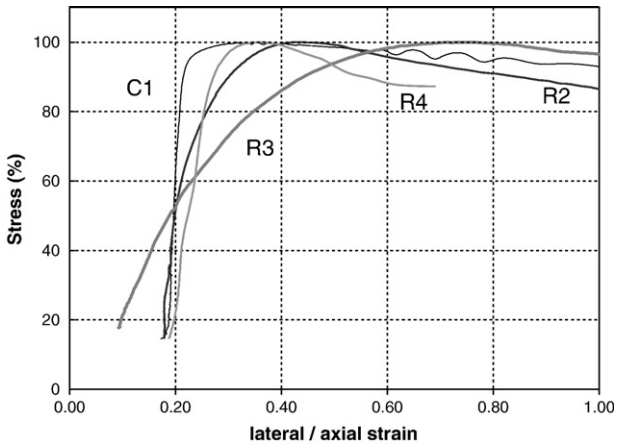

Fig. 6. Typical stress (%) vs. lateral/axial strain ratio of damaged and control concretes.

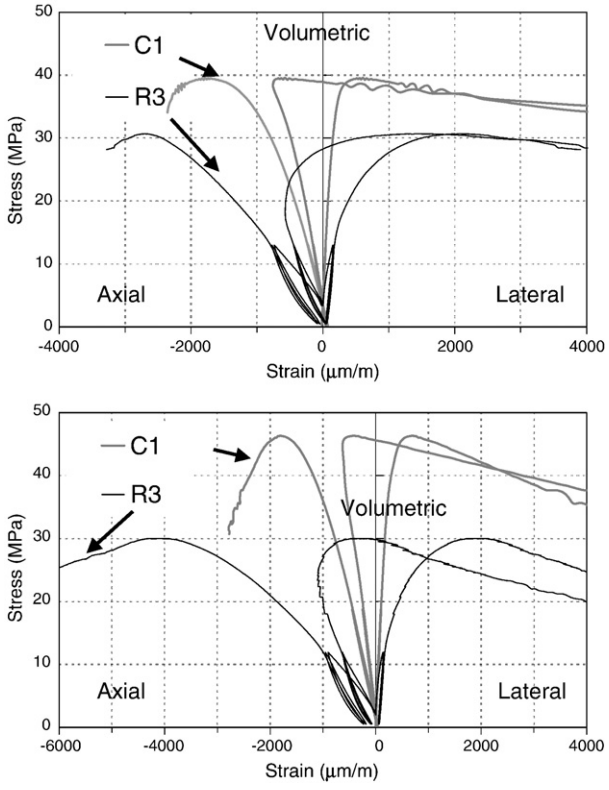

Fig. 7. Stress–strain curves in compression of damaged R3 and control concretes. Top: measured at 75 days, Bottom: measured at 120–250 days.

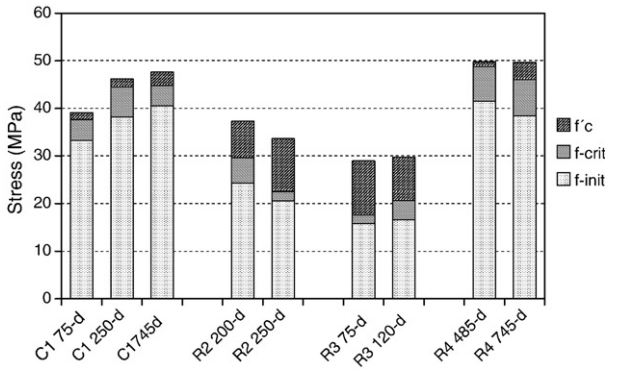

Fig. 8. Initiation and critical stresses and compressive strength.

concrete structure was observed. The gel is also found along the interfaces with non-reactive coarse aggregates, in discontinuities or unbounded zones. The gel located in pores mostly appears white in color, with numerous desiccation cracks due to loss of water and powder texture due to its carbonation. After 18 months the expansion achieved 0.295% indicating a progress in the deleterious reaction. The study of polished thin sections performed on samples obtained from the extremes and central part of the prisms shows a microstructural physiognomy similar to that previously explained. In addition, it was observed a greater grade of deterioration inside the reactive aggregates, microcracks starting inside the aggregates and running into the cement paste, increases their thickness achieving values near 0.06 mm. Gels present similar morphology, texture and location than those found at an earlier age (Fig. 2c).

Concrete R3 was prepared combining two types of coarse aggregates, 90% of non-reactive granite (C) and 10% of a very reactive orthoquartzite (A). In the case of aggregate A the typical reaction develops at the interfaces, it involves the dissolution of the cementing material of the rock, then the reaction rims are mainly located around the reactive aggregate; afterwards, the gel is expulsed toward the cement paste. Fig. 3 presents some polished and thin sections of concrete R3. Fig. 3a (obtained at the age of 30 days) shows clear manifestations of deleterious process. It can be seen that a wide reaction rim was produced by the dissolution of the siliceous cement of the orthoquartzite. A small crack into the aggregate and pores filled with gel appeared in the mortar. As time passes the deleterious manifestations increased. The observations performed at the age of 4 months (Fig. 3b and c) indicate that the reaction rims have grown, and gel migrates to more external sectors generating microcracks that run through the cement paste. Cracks usually are irregular, concentrated, orientated in parallel way and running through the cement paste and other fine and coarse aggregates that are close to the reactive aggregates. These cracks are wide, most of them achieve 0.08 mm opening, and they usually appear filled with gel.

The same as in concrete R2 the reaction kinetic is rapid. The drastic increase in dissolution of siliceous material of the rock and the great production of gel generates a great volume increase in a short time. As concrete cannot relax stresses and deformations exceed the extensibility of concrete, there only appear cracks of great width that start at the reactive interfaces and grow through the adjacent cement paste.

Concrete R4 was prepared with the reactive coarse aggregate B. The reactive mineral is polycrystalline strained quartz with clear signs of deformation, with slow or late expansion. An expansion of 0.100% at 15 months was measured. The reaction produces a slow dissolution and formation of gel in localized parts of the aggregates inducing a moderate expansion rate without significant signs of damage. The slow rate makes possible an internal stress relaxation leading to a formation of a diffused microcrack pattern, only manifested in thin sections. Fig. 4a shows a microcrack inside the reactive aggregate which appears widened by the local dissolution in its lips, produced when the thermodynamically unstable silica reacts with pore solution. One of the main characteristics of this reaction is the absence of reaction rims on the periphery of the aggregate; there are only few damaged zones at the interfaces, the attack being very punctual and in most cases no associated microcracks can be seen. It is difficult to establish a direct relationship between the reactive aggregate and the presence of microcracks filled with gel in the mortar, nevertheless exhaustive observations show a system of abundant microcracks distributed on the whole cement paste, with prevalent thickness ranging between 0.002 and 0.009 mm. Most of them are straight or slightly curved, usually empty, forming an interconnected net (Fig. 4b). Thin microcracks start inside the coarse reactive aggregates, grow as a consequence of gel expansion, and cross the interfaces in normal direction to penetrate into the cement paste. Image analysis using inverted light (Fig. 4c) shows an increase in microcracks width when they cross the cement paste probably due to its lower strength. Finally, in localized sectors of the cement paste, few microcracks filled with gel with irregular shapes and higher thickness (near 0.02 mm) were seen.

Table 4 presents typical characteristics of the crack pattern obtained from microscope observations. A survey of cracks located in the cement paste, into the reactive aggregate or at the interfaces was made. The density of cracks expressed as the total length per unit area is informed; considering that large defects have major influence on the failure mechanism of concrete the maximum crack width is also included. In concrete R4 wide and thin cracks in the cement paste were differentiated; it is clearly seen that the latter are prevalent. All concretes show similar maximum interface crack width, but concrete R3 also presents reaction rims with thickness up to 2 mm, note that the maximum width inside the aggregates is smaller in this case.

Summarizing, as previously described the selected reactive aggregates present a different kinetics of reaction in accordance with their composition. Then, the manifestations of ASR and the damage produced are quite different. The main differences are the rate of expansion, initiation and location of cracks, size of cracks, presence of gel in cracks and voids or development of reaction products (reaction rims) at the interfaces, among others.

In concrete R2 a general damage takes place due to ASR of the fine aggregates, the structure of concrete is affected by diffused microcracking showing the presence of gel in the periphery of sand grains. In concrete R3 local damage takes place on the periphery of the reactive coarse aggregates. The process is uniform enhancing a strong increment of the porosity on contour of the inclusions by loss of the cementitious components. At the same time the structure of concrete is damaged by the presence of interfaces and matrix cracks. In concrete R4 while the expansions indicate that there is ASR, damage can not be easily verified by the concrete microstructure observations. Non-extensive cracks or presence of reaction gel has been found. Expansion points in the bulk of the coarse aggregates, where pore solution accedes, induce stresses on the mass of concrete but do not necessarily produce big cracks probably due to some stress relaxation process.

3.2. Mechanical behavior

3.2.1. Failure mechanism in compression

The main results from compressive tests are given in Table 5. It includes the compressive strength ($f'c$), modulus of elasticity (E) and Poisson's ratio (μ), and, initiation (f_{init}) and critical (f_{crit}) stresses as significant parameters of the failure mechanism of concrete. The corresponding expansions obtained from 75×75×300 mm prisms tests data (Fig. 1) are also included.

It can be seen that, after 28 days, in concrete C1 the strength increases and the modulus of elasticity remains practically constant. In concretes R2 to R4 there are different behaviors.

There is almost no evolution in concrete R3. At the same time, it has lower stiffness than C1 that can be attributed to the presence of

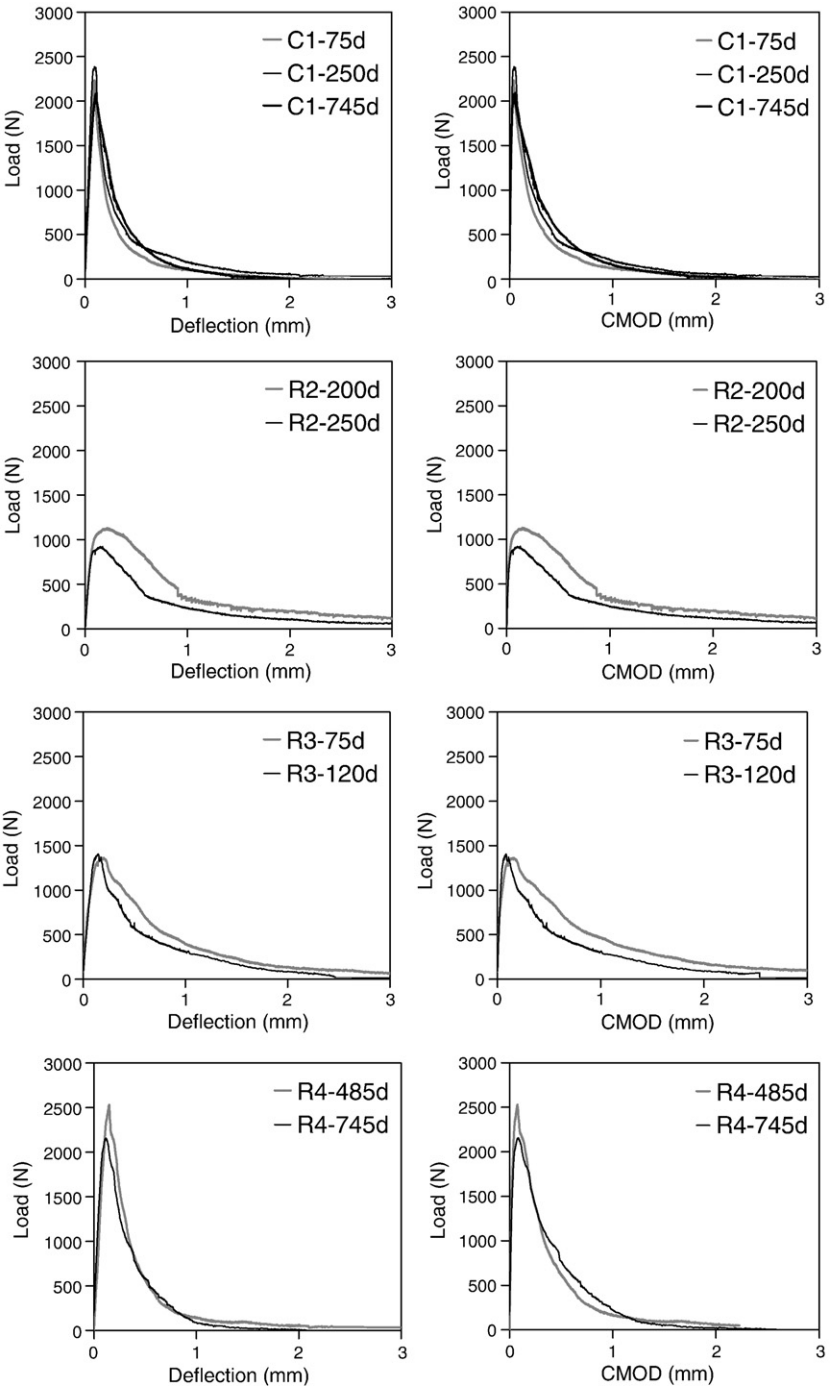

Fig. 9. a. Typical load-deflection and b. load-CMOD curves corresponding to control and reactive concretes.

the orthoquartzitic aggregate and to the degradation of the microstructure of concrete (note the decrease in the elastic modulus at 120 days in concrete R3). It must be noted that even at 75 days concrete R3 was markedly affected showing visible cracks on the specimen's surface, as a consequence no significant differences appear comparing 75 and 120 days test results.

Concrete R2 shows an increase in strength from 28 to 200 days. The existence of an ASR induction period of near 100 days, probably enables the strength evolution. After 200 days there is a clear decrease in strength. This fact was observed in both sizes of cylinders. It is very interesting to mention that at 200 days although the strength increases, the modulus of elasticity markedly decreases, showing the internal damage.

Concrete R4 increases strength up to near 1 year the same as C1. Nevertheless while the stiffness of C1 remains almost constant, the modulus of elasticity of R4 decreases near 20%.

A general analysis indicates that although the measured expansions were similar for concretes R2 to R4, the effects on strength and stiffness can be very different depending on the source of ASR damage.

The failure process in compression can be studied by means of the development of axial and lateral deformations as load increases [19]. Differences in crack pattern are reflected in the shape of curves and the typical parameters obtained, as critical stresses. Usually crack growth starts at the interfaces, propagates into the matrix and run around the aggregates. Coarse aggregates arrest crack propagation, resulting in multiple crack formation. When different types of aggregates or matrix

Table 6
Results form flexural tests

Concrete	Age	f_{net}	G_F	E[a]	f_s[b]	l_{ch}	Expansion[c]
	(days)	(MPa)	(N m)	(GPa)	(MPa)	(mm)	(%)
C1	75	6.0 (12)[d]	226 (9)	38.7	3.6	670	0.004
	250	7.6 (11)	233 (15)	39.7	4.5	450	0.007
	745	7.4 (13)	178 (13)	39.6	4.5	350	0.054
R2	200	3.3 (16)	330 (32)	19.9	2.0	1700	0.145
	250	3.0 (12)	242 (10)	12.1	1.8	900	0.180
R3	75	3.8 (12)	370 (16)	19	2.3	1370	0.115
	120	4.1 (10)	254 (20)	18.4	2.4	780	0.145
R4	485	6.0 (11)	204 (18)	33	3.6	510	0.125
	745	7.0 (8)	235 (10)	28.8	4.2	390	0.135

f_{net}: Flexural bending stress.
G_F: Energy of fracture.
f_s: Tensile strength.
l_{ch}: Characteristic length.
[a] From cylinders of 150×300 mm.
[b] Estimated as 0.6 f_{net}.
[c] Interpolated from Fig. 1 data.
[d] COV (%).

strength levels are used, cracks may also develop through the aggregates modifying the stress–strain curves [23]. In similar way when concrete presents extensive cracking, as when it is exposed to high temperature, the fissures lead to a marked non-linear behavior and the deformations strongly increase [24].

Fig. 5 compares typical stress–axial strain curves obtained for each ASR concrete for expansions between 0.135 and 0.145%, a curve for concrete C1 is also included. It can be seen that in R3 the axial deformation corresponding to maximum load achieves values near 4000 μm/m, twice a sound concrete. The stress–strain curves of concretes R4 and R2 are placed between C1 and R3. In addition it must be observed that the first part of the curves (first and third loading cycles) is different; when the damage increases (C1, R4, R2, R3) more significant inelastic strains develop. Note that even in R4 where the compressive strength is higher than in C1, there is an increase in the residual strains after unloading (up to 40%) indicating that internal damage was present before testing.

Fig. 6 shows the stress (in %) vs. lateral/axial strain ratio of damaged and control concretes presented in Fig. 5. The stress at which the lateral/axial strain ratio begins to increase is called initiation stress (f_{init}) and it is associated with crack formation in the mortar matrix. It can be observed that while in C1 the lateral/axial strain ratio remains almost constant beyond 80% of the compressive strength, the damage produced by ASR leads to a progressive increase of the lateral/axial strain ratio below 60% of $f'c$ in R3. The behavior of concrete R2 is close to that of R3 while R4 is more similar to C1.

Fig. 7 compares the axial, lateral and volumetric stress–strain curves of C1 and R3 at two ages. In concrete R3 the presence of cracks modifies the shape of the volumetric strain curve. At both ages damaged concrete clearly behaves in a non-linear way, this behavior being more marked at advanced ages when the degradation is more extensive. Based on the stress–volumetric strain curve is defined the critical stress (f_{crit}) (minimum peak of strains), which is associated with the onset of unstable propagation of cracks in the matrix of concrete. It can be seen that in R3 the critical stresses are near 65% of ultimate stress meanwhile in C1 they are higher than 90%.

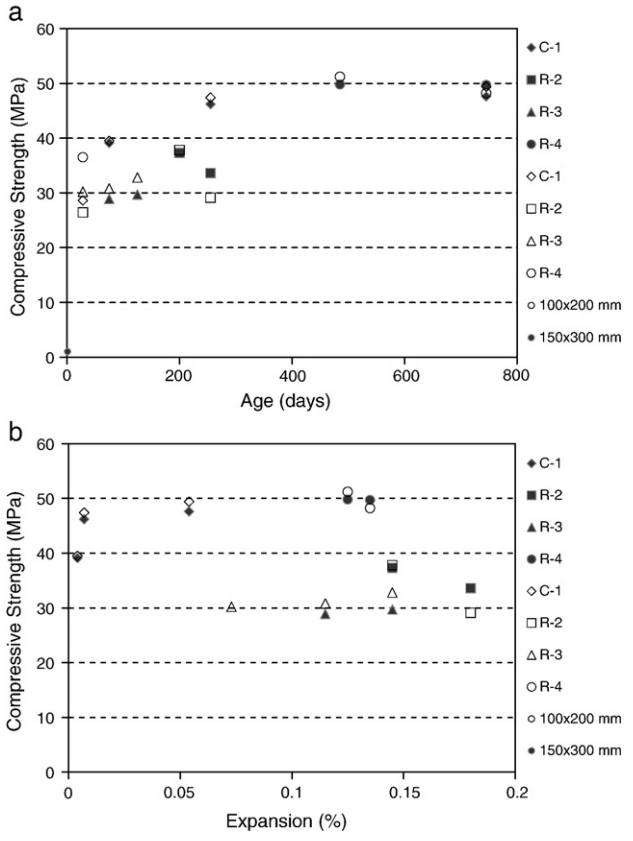

Fig. 10. a. Variation of compressive strength with age. b. Relationship between compressive strength and expansion.

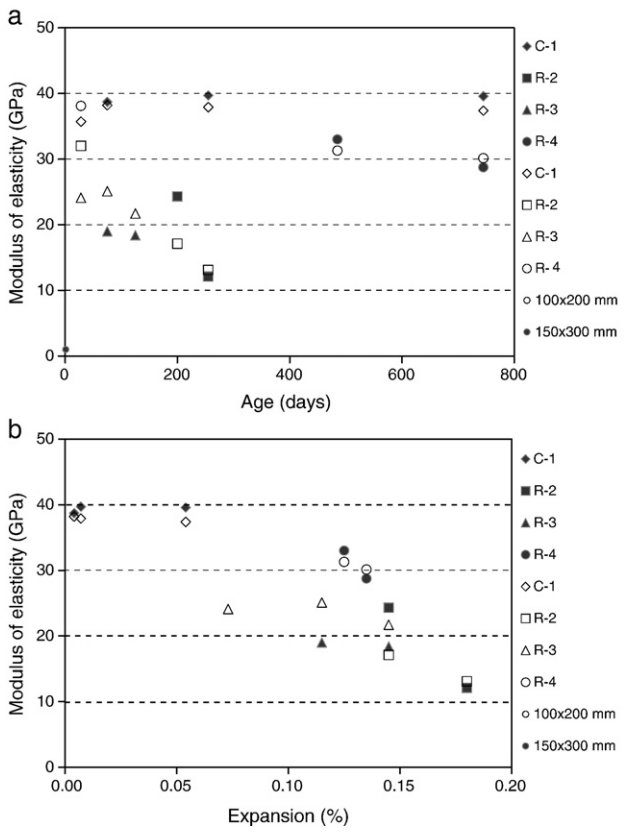

Fig. 11. a. Variation of modulus of elasticity with age. b. Relationship between modulus of elasticity and expansion.

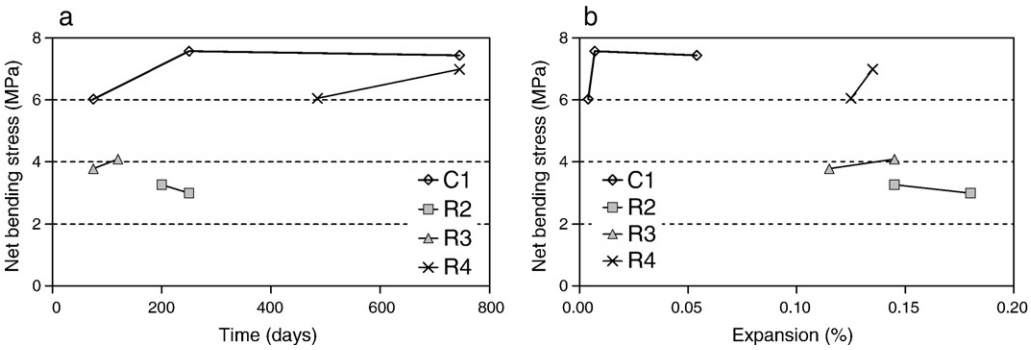

Fig. 12. a. (left) Variation of net bending stress with age. b. (right) Relationship between net bending stress and expansion.

When the ASR is diffused into the matrix (R2), a decrease in critical and initiation stresses and an increase in axial deformation were also measured. Comparing R2 and R3 it can be seen that while the measured expansion were higher in R2, the decreases in f_{init} and f_{crit} were greater in R3, indicating a different crack pattern. This observation is confirmed from test results of R4, where practically no effects on the failure mechanism parameters in compression ($f'c$, f_{init}, f_{crit}) were detected for expansions higher than 0.12% (see Figs. 5 and 6, and Table 5).

Summarizing the analysis of failure mechanism in compression, Fig. 8 compares the initiation stress, the critical stress, and the compressive strength. It can be clearly seen that the internal damage in concrete produced by ASR, leads to a decrease of f_{init} and f_{crit}. This means that, due to the cracking, the growth and propagation of matrix cracks start earlier. The period of stable crack propagation in the mortar (given by the difference between $f_{crit}-f_{init}$) is less affected than the period of unstable crack growth (given by the difference between $f'c-f_{crit}$) which is widely extended. The capability of controlling crack propagation decreases leading to premature failure and consequently lower strength. However, while the expansions measured on R2, R3 and R4 are comparable, the concrete failure mechanism in compression depends on the origin and kinetic of the reaction, and the consequent morphology of cracking.

3.2.2. Mechanical behavior in tension

The behavior of concrete in tension is presented in Fig. 9a and b, where typical load-deflection and load-CMOD curves are shown. The shape of the curves reflects the differences in the crack pattern between sound and damaged concretes. A linear behavior is seen up to peak load in concrete C1; the development of the cracks starts just before the maximum load is achieved. In this case although there is interface cracking before loading, the amount and magnitude is very limited.

In ASR damaged concrete extensive cracking is present before loading both at the interfaces and at the matrix. This is especially noted in concretes R2 and R3 which show an increased non-linearity before the peak and a more gradual softening in the descending branch. This behavior indicates that extensive meandering and branching of cracks is taking place in damaged concrete. On the contrary while similar expansion has taken place in R4, the shape of the load-deflection curves was similar to concrete C1. Fig. 9a and b shows minor differences in the shape of the curves of concretes C1 and R4 at later ages.

As a result of the differences in cracking process the energy of fracture and the size of the zone where this process takes place, will be strongly affected [25]. Table 6 presents the results of flexural bending stress in notched beams and the energy of fracture calculated from the load-deflection curves. The values of tensile strength and characteristic length are also included. It can be seen that in concretes R2 and R3, ASR lead to a reduction of flexural tensile strength near 40% compared with C1, which was, as expected, higher than the reduction observed in compressive strength (near 25%). However, tensile strength only decreased slightly in R4. Regarding the energy of fracture it was observed an increase in the COV (%) in damaged concretes. This can be attributed to the own heterogeneity of the ASR location.

Concretes C1 and R4 show similar values of the characteristic length, the general expansion at very slow rate that takes place in R4 has almost not effects on the size of the fracture zone. On the contrary in concretes R2 and R3 the size of the fracture zone markedly increases due to the extensive meandering and branching of cracks combined with the reduction in tensile strength and stiffness. In addition it can be seen a decrease in the characteristic length in concrete C4 with time, as it occurs with concrete C1.

4. Discussion

The mechanical response of concretes damaged by ASR has been compared with that of a sound concrete. As different types of reactive aggregates were used, the rate of degradation and the morphology of the internal damage were different, then crack pattern changes in each case.

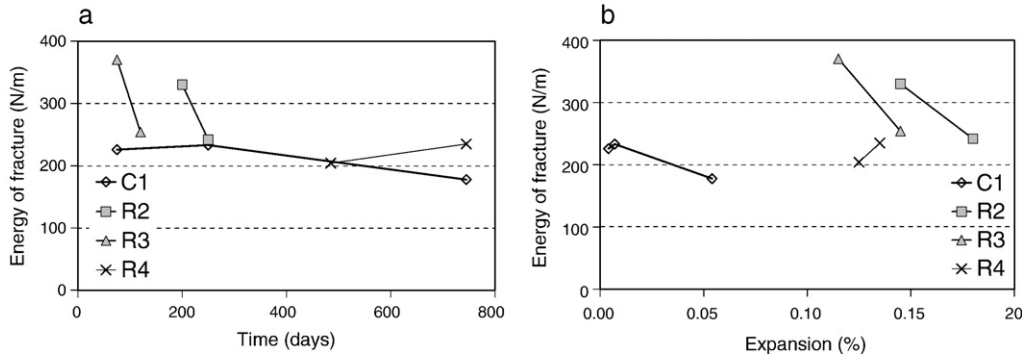

Fig. 13. a. (left) Variation of the energy of fracture with age. b. (right) Relationship between energy of fracture and expansion.

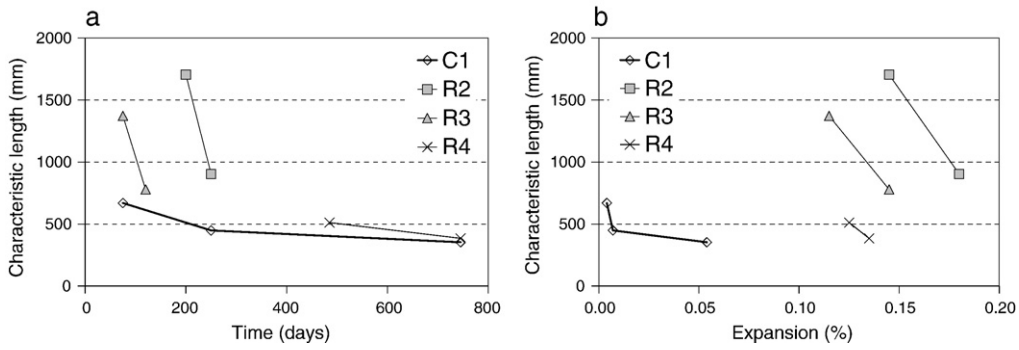

Fig. 14. a. (left) Variation of the characteristic length with age. b. (right) Relationship between characteristic length and expansion.

As it is usual, length changes were recorded to evaluate the damage due to ASR. High rate of degradation and stable values after 150 days were observed in concrete R3. In concrete R2 an induction period near 100 days was observed and after that a significant expansion develops. In concrete R4 the expansion slowly starts after more than 1 year. Mechanical tests and observations of the internal structure of concretes were performed when linear expansions higher than 0.110% were measured in concretes affected by ASR.

The compressive tests showed that, as it was expected, in reference concrete there is an evolution of strength after 28 days, whereas in concretes with great damage produced by ASR, there is no strength gain. It is very interesting to note that in the case of slow rate ASR (R4), no significant effects on compressive strength were found. In this case the attack is not generalized and the internal stresses are not always enough to develop significant cracking. Although there is significant density of cracks in the cement paste (Table 4) these cracks are very thin and they do not modify the failure mechanism and the mechanical response, with the exception of the modulus of elasticity.

Fig. 10a and b plots the results of compressive strength vs. time, and compressive strength vs. expansion; it can clearly be seen that a comparable expansion level not necessarily corresponds to a similar effect on compressive strength. In the same way Fig. 11a and b represents the variation of the modulus of elasticity; in this case the decrease in stiffness is in accordance with the increase in expansion.

The presented results show that the failure mechanism of concrete in compression is clearly affected by ASR damage. The shape of the stress–strain curves (axial, lateral and volumetric) reflects the presence of internal fissures. The variation of lateral/axial strain ratio with increasing loads also changes in significant way. In concretes R2 and R3, where significant cracking was generated by ASR, the growth and propagation of matrix cracks start earlier. The period of stable crack propagation is less affected than the period of unstable crack growth which is widely extended, showing that the capability of controlling crack propagation decreases leading to premature failure. However, the changes in the initiation or critical stresses in compression (Fig. 8) can not be easily related with the expansions measured on prisms (near 0.14% in R2 to R4).

The differences in the crack pattern of sound and damaged concretes are also reflected in the shape of the load-deflection curves in tension, both in the pre- and post-peak regime (Fig. 9). The most damaged concrete shows an increased non-linearity before the peak and a more gradual softening in the descending branch, which indicates that extensive meandering and branching of cracks is taking place. The extensive presence of cracks in the mortar and interfaces were associated with a decrease in strength and an increase in the size of the fracture zone (Figs. 12–14). Contrarily concrete R4, with a slow rate ASR coarse aggregate, shows no significant effects both on the energy of fracture and the tensile strength.

Considering that, as it is known, the size and extension of cracks directly affect the macroscopic response of the materials, Fig. 15 represents the relative values of the mechanical properties of concretes R2, R3 and R4, referred to C1, as a function of the level of damage. The mechanical parameters of concretes R2, R3 and R4 were considered in the most damaged state and in C1 at the age of 8 months. The level of damage is represented by the product of the crack maximum width and total length (MW.TL) indicated in Table 4. In R4 only wide cracks were considered. The effects produced by the cracks in cement paste, at interfaces and inside the aggregates are analyzed. When the fissures at the cement paste are considered, MWc.TLc, low values appear for R4, higher in R2 and the highest in R3; this agrees with the variation of the mechanical properties referred to C1. When interfaces cracks are analyzed again the low decrease of R4 is justified. Finally, regarding aggregate cracks, the greater number corresponds to R4 followed by R3 and R2, being no direct correlation with the mechanical properties.

Fig. 15 shows that the parameters representative of the failure in compression clearly decrease as the interface and bulk cement paste

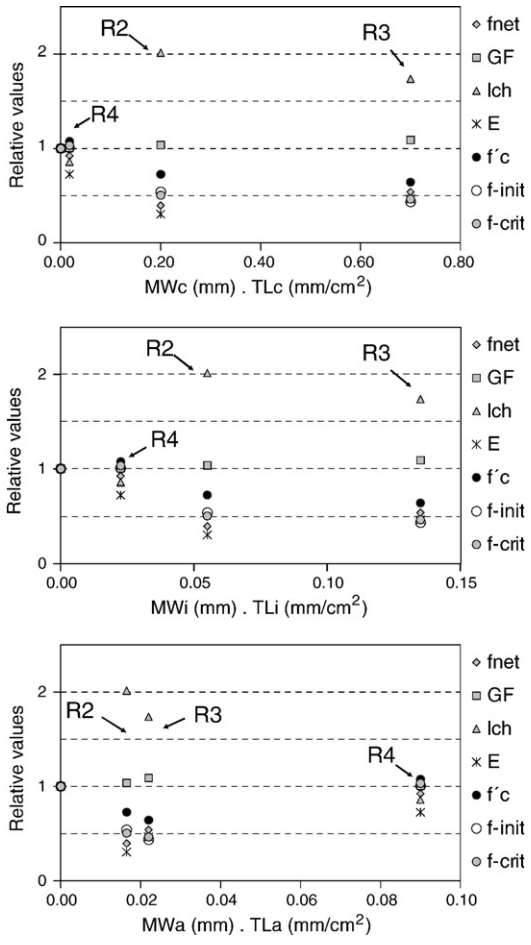

Fig. 15. Effect of crack pattern on the mechanical properties in concretes affected by ASR.

damage increase. In addition, thin microcracks affect more the stiffness than the strength (as can be seen in concrete R4). The relative net bending strength slightly decreases in R4 and in a more significant way in R2 and R3; however it can not be seen a direct relationship with MW.LT, as it is the lowest in R2, probably due to the presence of more disseminated defects. Regarding the other properties related with tensile behavior, there were found minor changes on the energy of fracture but while the size of the fracture zone does not change in R4 strongly increases in R2 and R3. The presence of big fissures produces a decrease in tensile strength but enhances the post-peak softening; the more diffused crack pattern in concrete R2 leads to greater values of l_{ch}, in the case of R3 the great defects at the interfaces enhance the meandering and branching of cracks.

The influence of ASR on mechanical properties of concrete is strongly dependent on the origin and kinetics of the reaction, and then, on the characteristics of crack pattern. Even for a similar expansion grade the effects on the failure mechanism can be very different.

5. Conclusions

The mechanical responses of concretes prepared with sound and ASR aggregates of different origin were studied. A highly reactive siliceous orthoquartzite as a part of the coarse aggregate, a reactive sand, and a slow reacting granitic coarse aggregate were used. The selected aggregates present differences in expansion rates, in the induction periods, signs of reaction and morphology of the damage.

Concrete prepared with the reactive siliceous orthoquartzite showed significant expansion during the first weeks, reaction products and dissolution zones in the rim of the rock, interface cracks and mortar cracks with and without gel. Concrete incorporating the reactive fine aggregate presents an internal structure affected by diffused microcracking showing the presence of gel in the periphery of sand grains. In concrete with slow ASR aggregates (granite with stressed quartz) damage is difficult to observe on the concrete microstructural analysis. This requires a sharp examination with stereo-zoom and polarizing microscope. Non-extensive cracks or presence of reaction gel has been found and a generalized degradation is assumed mainly initiated at localized zones on the bulk of the coarse aggregates, the lack of wide cracks could be justified assuming some stress relaxation process.

Mechanical tests were performed when damaged concretes achieved linear expansions between 0.11 and 0.18%. As expected there was an important compressive strength gain in reference concrete after 28 days. A different behavior was found in concretes including reactive aggregates. Concretes prepared with the rapid reactive aggregates show no strength gain, and significant reductions in the elastic properties (modulus of elasticity and Poisson's ratio). On the contrary, in concrete including the slow rate reactive coarse aggregate the compressive strength increases in comparable way as reference concrete, but the elastic properties are affected.

The failure mechanism of concrete in compression is clearly affected by ASR. The shape of the stress–strain curves reflects the presence of internal fissures. The growth and propagation of matrix cracks tends to start earlier due to defects produced by ASR. The period of stable crack propagation is less affected than the period of unstable crack growth which is widely extended, showing that the capability of controlling crack propagation decreases leading to premature failure.

As it occurs in compression, the differences in the crack pattern of sound and damaged concretes are reflected in the shape of the load-deflection curves, both in the pre- and post-peak regime. Damaged concretes show an increased non-linearity before the peak and a more gradual softening, which indicates that extensive meandering and branching of cracks is taking place. It was found that the variability in test results increases in concretes affected by ASR, especially when rapid reaction takes place.

The mechanical properties of concretes prepared with reactive aggregates decrease as the ASR develops. However, these experiences demonstrate that it is not easy to associate the changes in the mechanical properties with a level of expansion as these changes depend on the materials and mechanisms involved in the reaction as the mineralogy of the rock, the size of the aggregate (coarse or fine reactive aggregates) and kinetics of reaction (rate of expansion).

References

[1] T. Katayama, D. Bragg, Alteration of S–C–H and ASR gel in deteriorated concretes, Newfoundland, Canada, Proc. Int. Conf. on Concrete under Severe Conditions, Saporo, Japan, 1995, pp. 1165–1174, 2.
[2] T. Katayama, D. Bragg, Alkali-aggregate reaction combined with freeze/thaw in Newfoundland, Canada Petrography using EMPA, Proc. 10th ICAAR, Melbourne Australia, 1996, pp. 243–250.
[3] T.E. Stanton, Expansion of concrete through reaction between cement and aggregates, Proc. Am. Soc. Civil Eng. 66 (1940) 1781–1811.
[4] B. Fournier, M. Berubé, Alkali-aggregate reaction in concrete: a review of basic concepts and engineering implications, Can. J. Civil Eng. 27 (2) (2000) 167–191.
[5] A.S.C. Fava, R.J. Manuele, J.F. Colina, C.R. Cortelezzi, Estudios y experiencias realizadas en LEMIT sobre reacción que se produce entre el cemento y los agregados en el hormigón de cemento portland, Serie Técnica N 85, LEMIT, La Plata, Argentina, 1991, (in spanish) 40 pp.
[6] D. Mc Connell, R. Meilenz, W. Holland, K.T. Greene, Cement — aggregate reaction in concrete, ACI J. Proc. 44 (10) (1947) 93–128.
[7] P.E. Grattan Bellew, Test methodology and criteria for evaluating the potential reactivity of aggregates, Proc. 8th ICAAR, Kyoto Japan, 1989, pp. 279–294.
[8] O.R. Batic, J.D. Sota, Reacciones deletéreas internas, in: E.F. Irassar (Ed.), Durabilidad del hormigón estructural, Argentina, 2002, pp. 157–216, (in spanish).
[9] J.M. Ponce, O.R. Batic, Different manifestations of the alkali-silica reaction in concrete according to the reaction kinetics of the reactive aggregate, Cem. Concr. Res. 36 (6) (2006) 1148–1156.
[10] L. Monette, J. Gardner, P. Grattan-Bellew, Structural effects of the alkali-silica reaction on non-loaded and laded reinforced concrete beams, Proc. 11th ICAAR, Quebec, Canada, 2000, pp. 999–1008.
[11] T. Siemes, J. Visser, Low tensile strength older concrete structures with alkali-silica reaction, Proc. 11th ICAAR, Quebec, Canada, 2000, pp. 1029–1038.
[12] A.E. Jones, L.A. Clark, A review of the Institution of Structural Engineers Report: structural effects of Alkali-silica reaction (1992), Proc. 10th ICAAR, Melbourne Australia, 1996, pp. 394–401.
[13] K. Takemura, M. Ichitsubo, E. Tazawa, A. Yonekura, Mechanical performance of ASR affected nearly full-scale reinforced concrete columns, Proc. 10th ICAAR, Melbourne Australia, 1996, pp. 410–417.
[14] W. Koyanagi, K. Rokugo, Y. Uchida, H. Iwase, Deformation behavior of reinforced concrete beams deteriorated by ASR, Proc. 10th ICAAR, Melbourne Australia, 1996, pp. 458–465.
[15] C. Larive, A. Laplaud, M. Joly, Behaviour of AAR-affected concrete, experimental data, Proc. 10th ICAAR, Melbourne Australia, 1996, pp. 670–677.
[16] O.R. Batic, C.A. Milanesi, J.D. Sota, Effects of alkali silica and alkali carbonate rock reaction on aggregate mortar bond, 11 ICAAR, Quebec, Canada, 2000, pp. 1–10.
[17] O.R. Batic, J.D. Sota, C.A. Milanesi, R. Pavlicevic, C.R. Cortelezzi, Estudio de rocas graníticas de la provincia de Buenos Aires desde el punto de vista de la reactividad de los álcalis del hormigón, Revista Hormigón 33 (1999) 11–39 (in spanish).
[18] O.R. Batic, J.D. Sota, Search of reliable methods for detection of granitic aggregate reactive to ASR, Proc. 12th ICAAR, Beijing, China, 2004, pp. 243–250.
[19] S.P. Shah, S. Chandra, Critical stress, volume change, and microcracking of concrete, ACI Mater. J. 60 (1963) 575–588.
[20] RILEM TC-50 FMC determination of the fracture energy of mortar and concrete by means of three-point bend tests on notched beams, Mat. Struct. 18 (106) (1985) 285–290.
[21] G.V. Guinea, J. Planas, M. Elices, Measurement of the fracture energy using three-point bend tests: part 1 — influence of experimental procedures, Mat. Struct. 25 (148) (1992) 212–218.
[22] A. Hillerborg, Additional concrete fracture energy test performed by 6 laboratories according to a draft RILEM recommendation, Repot TVBM-3017 (Division of Building Materials, Lund Institute of Technology), 1984, 12 pp.
[23] G. Giaccio, C. Rocco, D. Violini, J. Zappitelli, R. Zerbino, High strength concretes incorporating different coarse aggregates, ACI Mater. J. 89 (3) (1992) 242–246.
[24] B. Barragán, A. Di Maio, G. Giaccio, L. Traversa, R. Zerbino, Effects of high temperature on residual mechanical and transport properties of concrete, in: V.M. Malhotra (Ed.), ACI SP-192, Fifth CANMET/ACI Int. Conference on Durability of Concrete, Barcelona, 2000, pp. 983–1000.
[25] B. Barragán, G. Giaccio, R. Zerbino, Fracture and failure of thermally damaged concrete under tensile loading, Mat. Struct. 34 (239) (2001) 312–319.